



Design of a resonant Luneburg lens for surface acoustic waves

Rafael Fuentes-Domínguez^{a,*}, Mengting Yao^a, Andrea Colombi^b, Paul Dryburgh^a, Don Pieris^a, Alexander Jackson-Crisp^c, Daniel Colquitt^d, Adam Clare^c, Richard J. Smith^a, Matt Clark^a

^a Optics and Photonics Group, Faculty of Engineering, University of Nottingham, Nottingham, NG7 2RD, UK

^b Department of Civil, Environmental and Geomatic Engineering, ETH, Stefano-Franscini-Platz 5, 8093 Zürich, Switzerland

^c Advanced Component Engineering Laboratory (ACEL), Faculty of Engineering, University of Nottingham, NG7 2RD, Nottingham, UK

^d Department of Mathematical Sciences, University of Liverpool, UK

ARTICLE INFO

Keywords:

Metamaterial
Luneburg lens
SAW
Additive manufacturing

ABSTRACT

In this work we employ additive manufacturing to print a circular array of micropillars on an aluminium slab turning its top surface into a graded index metasurface for surface acoustic waves (SAW). The graded metasurface reproduces a Luneburg lens capable of focusing plane SAWs to a point. The graded index profile is obtained by exploiting the dispersion properties of the metasurface arising from the well-known resonant coupling between the micropillars (0.5 mm diameter and variable length ~ 3 mm) and the surface waves propagating in the substrate. From the analytical formulation of the metasurface's dispersion curves, a slow phase velocity mode is shown to arise from the hybridisation of the surface wave with the pillar resonance. This is used to compute the radial height profile corresponding to the refractive index given by Luneburg's equation. An initial validation of the lens design, achieved through ray theory, shows that ray trajectories have a strong frequency dependence, meaning that the lens will only work on a narrow band. An ultrasonic experiment at 500 kHz where plane SAWs are generated with a piezoelectric transducer and a laser scanner measures the out of plane displacement on the metasurface, validates the actual lens performance and the manufacturing technique. Finally, comparison between the ray analysis and experimental results offers insight into the behaviour of this type of metasurface especially in the proximity of the acoustic bandgaps and highlights the possibility for acoustic shielding.

1. Introduction

The use of *metamaterials* to manipulate the propagations of waves has proven to be very successful, not only in electromagnetic devices where the research initially started [1,2], but also, more recently, in the field of mechanical waves [3,4]. Nowadays, a large number of structured materials fall into the metamaterial category, mainly because their microstructure can be ad-hoc engineered so that wave propagation may be precisely controlled. This is the case, for instance, with phononic crystals relying on Bragg scattering [5], composites working as effective media [6], and locally resonant materials relying on Fano-like interactions [7,8]. The concept of precise wave control using metamaterials is becoming central for several novel technologies, not only at the micro or centimetre scale typical of ultrasonics imaging, microfluidics, or acoustic noise abatement devices but also in mechanical and civil engineering. Here metaframes, large scale seismic metamaterials and building integrating resonant elements are currently being developed to exploit bandgaps, i.e. frequency bands where waves do not propagate. While bandgap has been the most exploited and

easy to control feature of metamaterials, precise wave control includes guiding, steering, beaming and focusing of mechanical waves. Experimentation on these advanced phenomena is conveniently carried out in small-scale proof of concept laboratory experiments at ultrasonic frequencies, possibly exploiting the flexibility of additive manufacturing as we do in this study. Insights can be easily translated to larger scales, lower frequencies, more complex models and different applications as witnessed for instance by a recent large scale experiment on seismic metamaterials [9] and on a vibration energy harvesting demonstrator for low frequency ambient noise [10]. Both studies have been inspired by ultrasonic experiments.

This work focuses on a particular type of metamaterial design, known as *resonant metasurfaces* [11–13], where clusters of subwavelength (local) resonators are arranged on an elastic surface such as a thin plate or a halfspace. It is well known that the interaction between surface waves propagating in the substrate and the local resonators produces bandgaps, and low velocities modes that can be exploited to build

* Corresponding author.

E-mail address: ezzf1@nottingham.ac.uk (R. Fuentes-Domínguez).

devices characterised by a custom refractive index (e.g. lenses) [14–17]. For instance, if we consider a metasurface made of longitudinally resonating rods interacting with surface acoustic waves (SAW), the so-called avoided crossing phenomenon [18,19] splits the otherwise continuous dispersion curves in two branches. In particular, the lower branch shows a gentle slope approaching the resonant frequency. This is the hallmark of “slow waves” travelling at a much lower speed than the surface mode in the homogeneous case [20].

Graded index lenses (GRIN) using a smooth refractive index transition throughout the lens, and have been studied since Maxwell’s early works [21]. Compared to standard lenses, GRIN lenses can steer the ray trajectory in smooth curves and avoid reflections. Examples of GRIN lenses are, for instance, flat lenses [22] and circular Luneburg, Maxwell and Eaton lenses [23,24].

For practical applications, the circular Luneburg lens, capable of focusing a beam of parallel rays (a plane wave) into a point on its opposite surface, is of particular interest as it requires “only” a 30% variation of refractive index, from the outside to the centre. This is much lower compared to the Eaton lens, which can be designed as an auto-reflector, but requires a 500% variation of the refractive index and therefore more extreme material properties [24,25].

GRIN lenses require a method of continuously varying the wave velocity as a function of position. Metamaterials with spatially graded properties are ideally suited for this purpose, with two alternative approaches currently available: The first relies on effective material properties given by non resonant inclusions aimed at increasing and decreasing the local density and stiffness respectively [26–29]. While this approach has the major advantage of being broadband, it requires a great deal of engineering to embed precisely softer or denser inclusions in the targeted component and might compromise its functionality. For several applications in ultrasonic imaging and mechanical energy harvesting one has access only to the medium surface and not its’ subsurface. In these instances, resonant metalenses can be easily obtained through surface patterning [13], a procedure made easier by the recent developments in the field of additive manufacturing. An example of potential application of patterned graded metasurface is given by vibration absorption based on the acoustic black hole (also a GRIN device) effect [30], currently limited to plate and obtained by tapering the thickness. The use of 3D printing and graded resonators would allow this device to be extended to thick elastic substrate.

There is a resounding lack of experimental studies in the field of resonant metalenses. The handful of research projects currently available in the literature are limited to numerical simulations. The first deals [25] with axisymmetric modes in thin plates while the most recent one by Palermo et al. [31] proposes a Luneburg lens for guided Love waves in a stratified halfspace endowed with in-plane resonators. Drawing on the analytical study by Colquitt et al. [12], that derived closed form solutions of the dispersion curves for metasurfaces made of rods on plates and elastic halfspaces, we design a resonant metalens for surface acoustic waves (analogous to Rayleigh waves in larger scale problems such as those in civil engineering). The surface of a commercial, 3 cm thick slab of aluminium is patterned through metal 3D printing with aluminium microrods. By exploiting the slow wave branch characteristic of the dispersion curves, the rod height profile equivalent to the refractive index profile of a Luneburg lens is obtained and validated using ray theory and ultrasonic experiments. We also explore the quality of the focusing and the losses in the bulk due to scattering.

2. Design of the acoustic Luneburg lens

A Luneburg Lens is a GRIN type lens and it can focus incoming waves on the opposite side of the lens with negligible loss and aberration. The lens refractive index can be described by the following equation:

$$n = \sqrt{2 - \left(\frac{r}{R}\right)^2} \quad (1)$$

Table 1
SAW Luneburg lens parameters and mechanical properties of aluminium.

Symbol	Definition	Value
L	Lattice spacing	2 mm
ρ	Density	2700 kg/m ³
μ	Shear modulus	26 GPa
λ	First Lamé parameter	58 GPa
d	Resonator diameter	0.5 mm
S	Resonator area	0.1963 mm ²
E	Young’s modulus	69 GPa

where R is the radius of the lens and $0 \leq r \leq R$.

For a 45 mm radius lens, Fig. 1(a) shows the refractive index distribution where the maximum value ($\sqrt{2}$) is at the centre ($r = 0$) and decays towards the edge of the lens ($r = R$).

The refractive index is the ratio of the speed of light in vacuum divided by speed of light in the medium. We can apply this idea to surface acoustic waves by converting this refractive index into the effective wave velocity inside the lens, $n = \frac{v_0}{v}$, where v_0 is the velocity of the waves without the lens. This velocity map is shown in Fig. 1(b) where the minimum velocity is obtained at the centre of the lens.

The design of the SAW Luneburg lens follows the same approach as the rainbow metawedge [13]. Firstly, the characteristics of the metasurface are explored considering an infinite periodic array of resonators with identical height, diameter of 0.5 mm and spacing between resonators of 1.5 mm. Periodicity enables one to use Bloch theory to consider a single resonator in a cell with Bloch periodicity condition on the lateral boundaries of the cell. The resulting dispersion curve relating phase shift across the cell to frequency is calculated using a 2D analytical approach that couples the longitudinal motion of the rods with the full Navier elasticity equations in the halfspace [12].

The dispersion relation of a linear array of resonators on an elastic half-plane can be obtained by solving numerically the following equation (3.27, from Ref. [12]).

$$4\xi\sqrt{\xi^2 - r^2}\sqrt{\xi^2 - 1} - (2\xi^2 - 1)^2 = \sqrt{\xi^2 - r^2} \frac{V(\omega)}{\omega L^2 \sqrt{\mu\rho}} \quad (2)$$

where the normalised variables are defined as $\xi = k/\Lambda_s$ and $r^2 = \Lambda_c^2/\Lambda_s^2 = 1/(2 + \lambda/\mu)$. $V(\omega) = S\omega\sqrt{E\rho}\tan(l\omega\sqrt{\rho/E})$ is the vertical force exerted on the half plane by the resonators and depends on the resonators height. All the parameters definition and values are described in Table 1.

Therefore, the dispersion curves for a range of rod heights are calculated (1–5 mm). These can be seen in Fig. 1(d). If we select a single frequency (500 kHz) for the lens design, we can convert rod height to acoustic velocity for that frequency which is shown in Fig. 1(e). Then, we can convert this into an equivalent refractive index by dividing by the wave velocity and use this with the Luneburg lens design equation (Fig. 1(f)). For this specific design, the bandgap is reached when the rods are larger than 2.5 mm; i.e., the value of the velocity tends asymptotically to 0.

Finally, by combining the dispersion curves for different rod heights at 500 kHz and the velocity map obtained by the refractive index formula, we can calculate the rod height profile necessary to design a Luneburg lens for SAW. The tallest rods are located in the centre of the lens, while the shortest at the edge. It needs to be noted that the diameter and spacing of the resonators are constant over the whole surface of the lens (see Table 1).

3. Ray tracing approach

To study the behaviour of the designed Luneburg lens, a ray tracing approach is used here [32]. This numerical method for tracing rays through graded-index media requires much less computational effort for obtaining a desired accuracy in comparison with existing methods such as finite element models. It can also provide information about

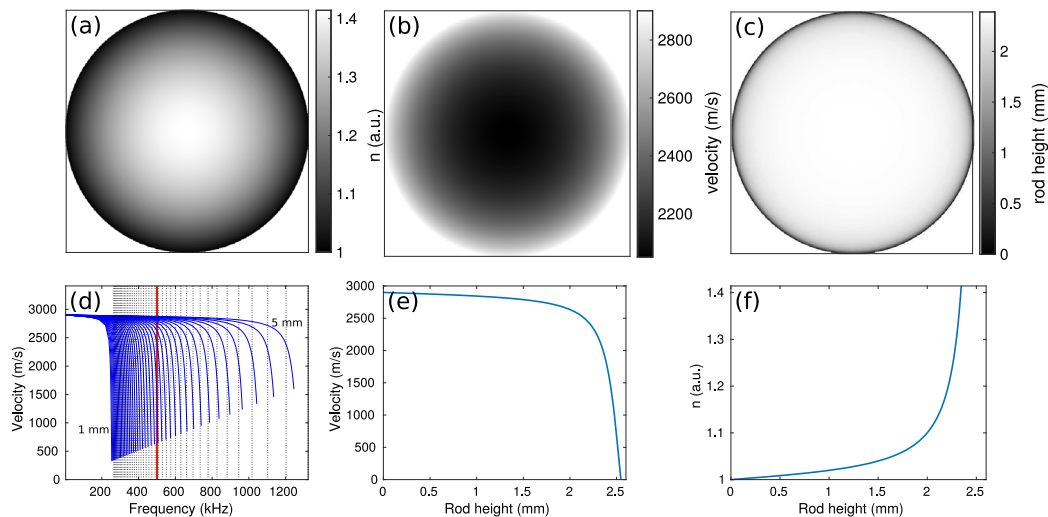


Fig. 1. Design of the SAW Luneburg lens. (a) is the refractive index of the lens given by Eq. (1). (b) is the velocity map obtained directly from the definition of refractive index, $n = \frac{v_0}{v}$, where v_0 is the SAW velocity in aluminium (~ 2900 m/s). (c) is the rod height map given by the dispersion curves for a fixed frequency of 500 kHz. (d) is the relationship between velocity and frequency for different rod height. (e) and (f) are the relationship between velocity and refractive index with respect to rod height, respectively, at 500 kHz.

the direction of the acoustic energy at each frequency, allowing a full understanding of the behaviour of the acoustic Luneburg lens. This is shown in Fig. 2 where the simulations for a 45 mm Luneburg lens at different frequencies are plotted. The parameters of the acoustic lens are obtained from Fig. 1(c) and Table 1.

From Fig. 2, information about the ideal performance of the SAW Luneburg lens can be extracted at different frequencies. For a lower frequency than the designed one, the focusing effect of the lens is insignificant or very weak. This can be seen at 450 kHz where the relative refractive index of the lens is less than 1.1 and the rays focus far from the edge of the lens. For the desired frequency, the SAW Luneburg lens works ideally, focusing the waves on the opposite edge of the lens. This is shown by the 500 kHz plot. When the frequency is beyond the desired one, the waves are focused before the edge as it can be seen at 530 kHz. If the frequency is increased more (around 540 kHz), an odd effect can be seen where some rays are focused in the centre of the lens and others are reflected. Finally, the bandgap is reached around 550 kHz where the wave is stopped and cannot travel through the lens, producing a shielding effect.

The plots from Fig. 2 will be shown experimentally with the designed Luneburg lens and using a broadband acoustic source with 500 kHz central frequency.

4. Experimental results

The sample was fabricated by selective laser melting (SLM) [33]. The ultrasound was generated by using a Panametrics Videoscan V414 0.5 MHz plane wave transducer with a 65° polymer wedge to couple the longitudinal wave of the transducer into a surface acoustic wave on the sample. The transducer and the wedge were glued to the sample using phenyl salicylate which provided good coupling and long term stability. The transducer was driven by a Ritec RPR-4000 programmable pulser using a 3-cycle sinusoidal burst at 500 kHz with an amplitude of 260 V peak-to-peak and repetition rate of 500 Hz. At this repetition rate, all echoes from the previous pulses were able to die out before the next measurement. The surface displacement due to the surface acoustic wave was measured by a rough-surface capable optical detector, Quartet LTG (Bossanova) in a single point (Fig. 3). Each single point consists of a 500 μ s time trace with 20 ns time steps. The signal was captured using a digital oscilloscope and averaged 100 times before transfer to a desktop computer. The sample was mounted on scanning stages and scanned over an area of 130 \times 110 mm with a step-size of 0.5 mm.

The raw data was filtered by a moving time window of 12 μ s to remove signals resulting from any undesired reflections from the edge of the sample. Fig. 4 shows the experimental results of the wave travelling through the Luneburg lens at different times measured by the rough-surface capable optical detector. It can be seen that the SAW is affected by the lens and is focused at the edge of the lens (as the ideal performance) between 90 and 120 μ s. This can also be seen in the finite element simulation included in the Supplementary Material. Although the programmable pulser generated a 3 cycle sinusoidal burst at 500 kHz, it can be seen how the group envelope is expanded due to the high dispersion inside the lens.

Although it is clear that the Luneburg lens behaves as expected (focusing the SAW at the edge), the plane wave generated by the 3 cycles sinusoid has a wide bandwidth. To extract individual frequencies and compare with the ray tracing approach, we firstly filtered the experimental signal to get a clean time domain signal at each point, then applied FFT to extract frequency signal (with 2 kHz frequency resolution), the phase map is the phase angle results after analysing the complex FFT results. This is shown in Fig. 5 where the amplitude and phase for 450, 500, 540 and 550 kHz are compared with the ray tracing model.

For the 450 kHz case, the experimental waves travel through the lens without being affected as it is shown by the very low spectral amplitude and flat waveform in Figs. 5(a) and (b), respectively, whose behaviour matches the ray tracing prediction.

At the target frequency (500 kHz), the spectral amplitude, 5(d), shows that the lens confines the energy at a very small zone at the edge of the lens. Also, shown in Fig. 5(e), the wavefronts are flat when they firstly travel into the lens, as the waves propagating, the bending effect appears. The wavefronts are much closer together inside the lens than the outside region, hallmark of a progressively lower wavespeed in the lens. In this case amplitude and phase results match the ray tracing result perfectly.

For the 540 kHz case, the spectral amplitude (Fig. 5(g)) shows that most of the energy is confined inside the lens, the incident waves cannot be transmitted. The phase, 5(h), shows an odd region at the centre of the lens. In the ray tracing result (i), most traces are confined inside the lens and only a few traces managed to escape, which agrees with the experimental results.

The 540 kHz frequency case is a regime with very strong scattering (seen in Fig. 5(g)), which makes it difficult to compare with the ray tracing. This is a case where ray tracing may give misleading information. While a solution to the ray equation still exist for all radii at this

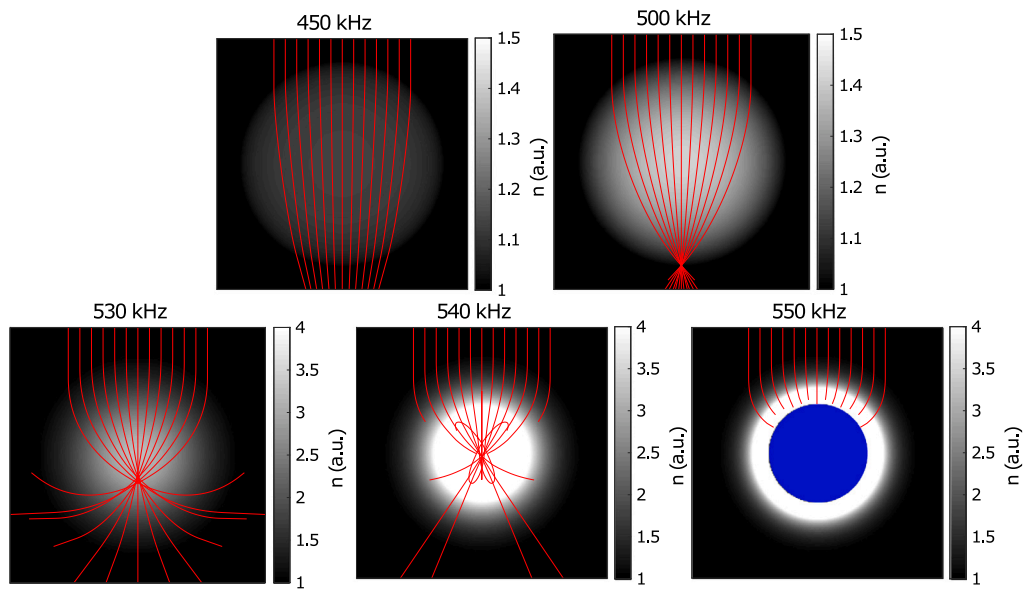


Fig. 2. Raytrace simulation of the 45 mm radius Luneburg lens at different frequencies. For a 450 kHz frequency which is lower than the designed frequency, the Luneburg lens has a lower refractive index and the SAW is slightly focused far from the edge of the lens. At 500 kHz (the target frequency), the wave is focused at the edge of the lens. At 530 kHz, the wave is focused inside the lens. If the frequency is increased and before reaching the bandgap, the raytracing simulation shows an odd behaviour at 540 kHz. Finally, the blue region contains the bandgap which appears around 550 kHz and the wave cannot travel through the Luneburg lens. (For interpretation of the references to colour in this figure legend, the reader is referred to the web version of this article.)

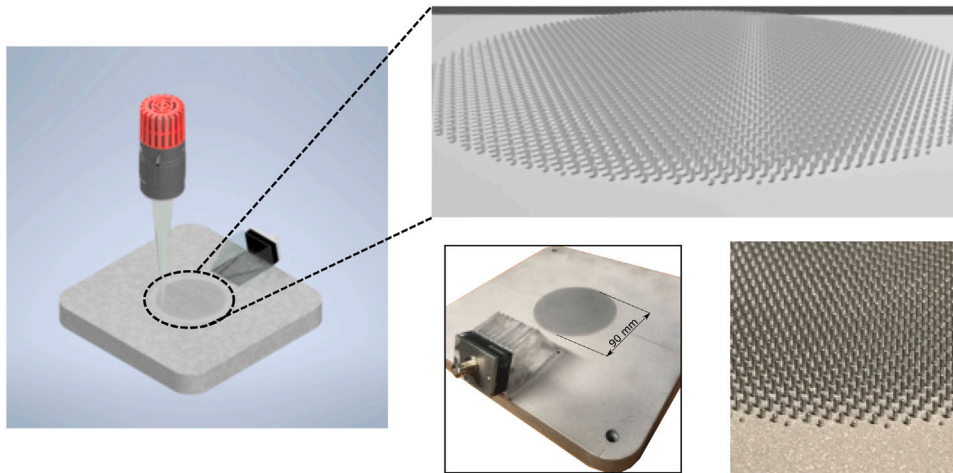


Fig. 3. The Luneburg lens on the surface of the aluminium block was mounted on electromechanical stages, a rough-surface capable optical detector, Quartet LTG (Bossanova) was used to scan the sample. The SAWs were generated and coupled by a transducer and polymer wedge. The resonator heights vary from 0.5 to 2.4 mm, with fixed 0.5 mm diameter, and their separation is 1.5 mm according to the design.

frequency, in practice waves cannot penetrate in the inner region because of the strong velocity gradient resulting in an abrupt impedance mismatch. This initially cause a focusing followed by reflection (or conversion in the resonators). By increasing the frequency, the whole inner region of the lens is located in the bandgap (vanishing velocity) and the signal is mainly scattered back and sideways.

For the 550 kHz case, the bandgap affects the propagation and rays are stopped and cannot go through the lens. In the experimental results, the bandgap effect can be observed as expected. The amplitude map 5(j) shows that there is no energy in the lens except for a thin ring around the edge, the inner part is perfectly shielded from the wave pulses. This is also shown by the phase plot with a similar ring shape phase distribution around the lens.

We see the energy flow simply stops in the previous pictures because of the spatial-temporal filtering. Making observations outside of these filter windows combined with observations of other similar objects indicated the energy is scattered after a relatively long period of time

(compared with the transit time of the main pulse). Essentially the energy is stored briefly in the resonant pillars near the bandgap and the re-radiated back out. We also observe the energy creeping along the bandgap. The details appear to be a complicated function of the shape, angle of incidence and the pseudo-crystal structure of the pillars making up the lens.

Finally, we have measured the focusing efficiency with respect to the frequency at different regions along the Luneburg lens: before the lens, inside the lens and at the focal point. Fig. 6(a) shows the average signal amplitude for the three different regions where a maximum peak is located at 500 kHz for the focal point and it is equivalent to a focusing efficiency of 250% (Fig. 6(b)).

5. Conclusions

We have shown the design, modelling and experimental results of a SAW Luneburg lens to focus incoming waves with negligible loss and

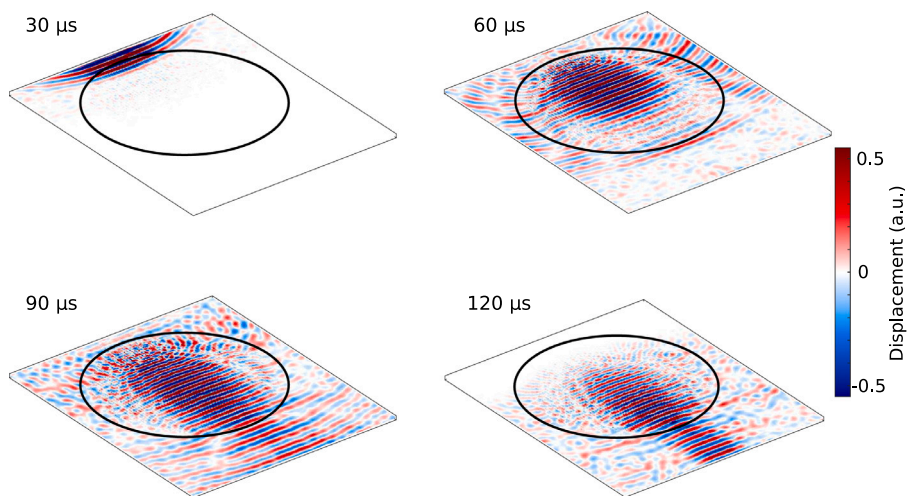


Fig. 4. Experimental results of the generated surface acoustic wave travelling through the Luneburg lens at different times: 30, 60, 90 and 120 μ s, respectively. It can be seen clearly that the acoustic waves is focused at the edge of the lens at 120 μ s.

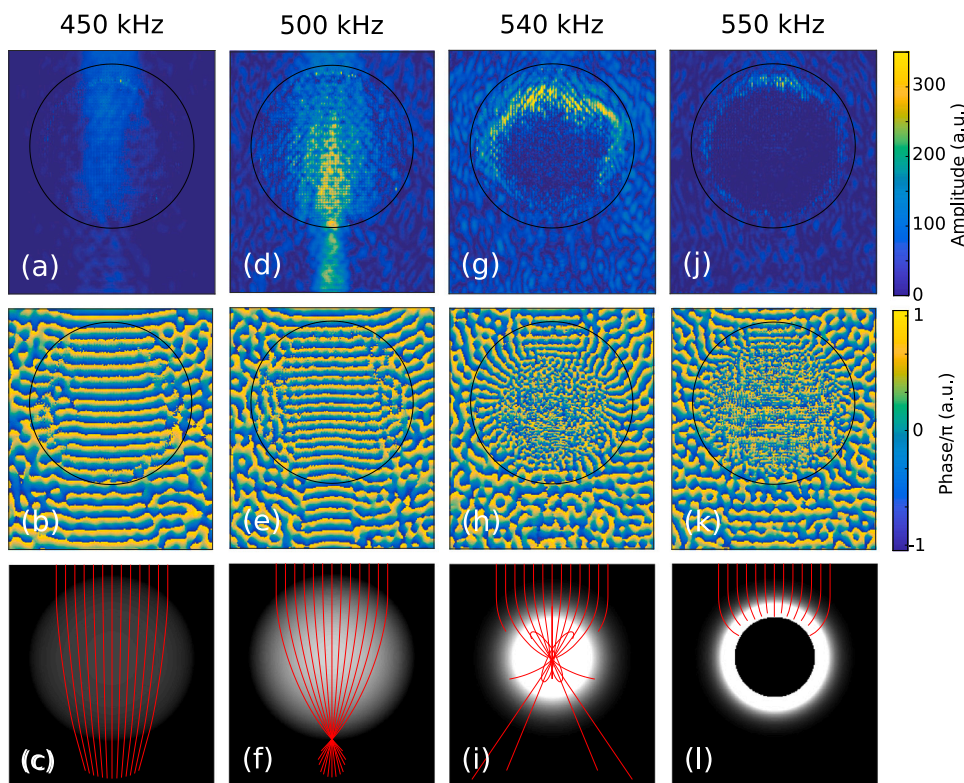


Fig. 5. This shows the fast Fourier transform (FFT) amplitude (top row), FFT phase (centre row) and ray tracing (bottom row) for four different frequencies. (a)–(c) are the case for 450 kHz which is lower than the ideal design, and where the acoustic wave is not much affected by the Lunenberg lens. (d)–(f) are the data for a frequency of 500 kHz, showing the focusing effect at the edge of the lens. (g)–(i) show the experimental data for 540 kHz frequency. (j)–(l) are the plots for a frequency of 550 kHz, showing that the acoustic wave is stopped by the bandgap.

aberration. The metalens was designed by combining the dispersion curves for different rod height at 500 kHz to match the refractive index map of a Luneburg lens. Then, the lens was modelled following a ray tracing approach which requires much less computational effort for obtaining a desired accuracy in comparison with finite element models. Furthermore, this analytical model allows one to study the behaviour of any metamaterial design for multiple frequencies. Additive manufacturing by SLM of aluminium micropowder proven to be very accurate despite the narrow tolerances of the model (0.5 mm pillar with height variation between rod down to 0.1 mm).

Although our ray tracing approach provides a very fast way to compute the behaviour of the Luneburg lens for different wavelengths, it cannot evaluate the focusing efficiency, the ultrasonic pressure or intensity gain and is only limited at the surface.

Finally, the experimental results show that the designed metalens focuses the incoming waves at the edge of the lens (as the ideal case) and also, the results match the ray tracing simulations for frequencies below and above 500 kHz. Lower frequencies are not affected by the lens, whereas higher frequencies waves are focused inside the lens until the bandgap is reached. In this case, the lens acts as perfect shield and

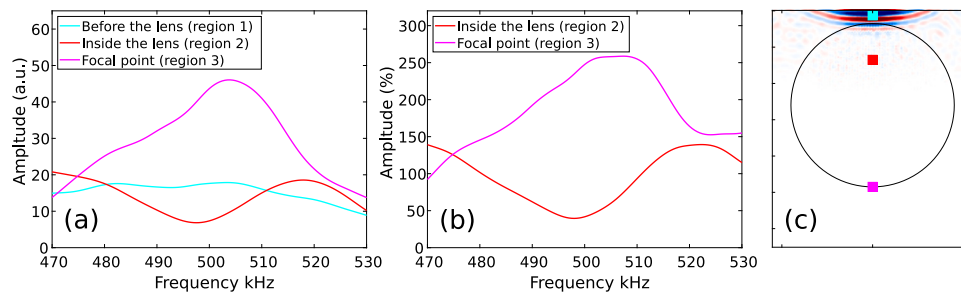


Fig. 6. This shows the focusing effect of the SAW Luneburg lens at different frequencies in three different locations: before the lens, inside the lens and at the focal point. (a) is the average signal amplitude where the maximum amplitude is located at the focal point at 500 kHz. (b) is the normalised signal amplitude with respect to the input signal where a 250% enhancement is seen at the focal point around 500 kHz. (c) shows the regions where the averaged signal was calculated.

the SAW cannot penetrate. The energy in this case is partially reflected backward and scattered in the bulk. In the medium term we believe that the control capacity of graded metasurfaces combined with the flexibility of fabrication via additive manufacturing is likely to impact future research in the field of microfluidic, ultrasonic imaging and vibration energy harvesting where precise wave control and focusing are of paramount relevance.

Declaration of competing interest

The authors declare that they have no known competing financial interests or personal relationships that could have appeared to influence the work reported in this paper.

Acknowledgements

This work was supported by the Engineering and Physical Sciences Research Council, UK [grant number EP/K021877/1]. A. Colombi thanks the SNSF, Switzerland for their support through the Ambizione fellowship PZ00P2-174009.

Appendix A. Supplementary data

Supplementary material related to this article can be found online at <https://doi.org/10.1016/j.ultras.2020.106306>.

References

- [1] J. Pendry, A.J. Holden, D.J. Robbins, W.J. Stewart, Magnetism from conductors and enhanced nonlinear phenomena, *IEEE Trans. Microw. Theory Tech.* 47 (11) (1999) 2075–2084.
- [2] S. Maier, K. Shamonina, S. Guéneau, O. Hess, J. Aizpurua, *Handbook of Metamaterials and Nanophotonics*, Vol. 2, World Scientific, Singapore, 2018.
- [3] M. Wegener, *Metamaterials beyond optics*, *Science* 342 (6161) (2013) 939–940.
- [4] S. Maier, K. Shamonina, S. Guéneau, O. Hess, J. Aizpurua, *Handbook of Metamaterials and Nanophotonics*, Vol. 1, World Scientific, Singapore, 2018.
- [5] N. Kaina, M. Fink, G. Lerosey, Composite media mixing Bragg and local resonances for highly attenuating and broad bandgaps, *Sci. Rep.* 3 (2013) 3240.
- [6] G. Milton, *The Theory of Composites*, first ed., Cambridge University Press, 2002.
- [7] A.E. Miroshnichenko, S. Flach, Y.S. Kivshar, Fano resonances in nanoscale structures, *Rev. Modern Phys.* 82 (2010) 2257–2298.
- [8] F. Lemoult, N. K., M. F., G. Lerosey, Wave propagation control at the deep subwavelength scale in metamaterials, *Nat. Phys.* (1) (2012) 55–60.
- [9] M. Lott, P. Roux, S. Garambois, P. Guéguen, A. Colombi, Evidence of metamaterial physics at the geophysics scale: the METAFORÉ experiment, *Geophys. J. Int.* 220 (2) (2019) 1330–1339.
- [10] J.M.D. Ponti, A. Colombi, R. Ardito, F. Braghin, A. Corigliano, R.V. Craster, Graded elastic metasurface for enhanced energy harvesting, *New J. Phys.* 22 (1) (2020) 013013, <http://dx.doi.org/10.1088/1367-2630/ab6062>.
- [11] J.B. Pendry, L. Martin-Moreno, F. Garcia-Vidal, Mimicking surface plasmons with structured surfaces, *Science* 305 (2004) 847–848.
- [12] D. Colquitt, A. Colombi, R. Craster, P. Roux, S. Guenneau, Seismic metasurfaces: Sub-wavelength resonators and Rayleigh wave interaction, *J. Mech. Phys. Solids* 99 (2017) 379–393.
- [13] A. Colombi, V. Ageeva, R.J. Smith, A. Clare, R. Patel, M. Clark, D. Colquitt, P. Roux, S. Guenneau, R.V. Craster, Enhanced sensing and conversion of ultrasonic Rayleigh waves by elastic metasurfaces, *Sci. Rep.* 7 (1) (2017) 6750.
- [14] Y. Achaoui, A. Khelif, S. Benchabane, L. Robert, V. Laude, Experimental observation of locally-resonant and Bragg band gaps for surface guided waves in a phononic crystal of pillars, *Phys. Rev. B* 83 (10) (2011) 10401.
- [15] Y. Xiao, J. Wen, X. Wen, Flexural wave band gaps in locally resonant thin plates with periodically attached springmass resonators, *J. Phys. D: Appl. Phys.* 45 (19) (2012) 195401.
- [16] N. Boechler, J. Eliason, A. Kumar, A. Maznev, K. Nelson, N. Fang, Interaction of a contact resonance of microspheres with surface acoustic waves, *Phys. Rev. Lett.* 111 (3) (2013) 036103.
- [17] M. Lott, P. Roux, Locally resonant metamaterials for plate waves: the respective role of compressional versus flexural resonances of a dense forest of vertical rods, in: *Fundamentals and Applications of Acoustic Metamaterials*, John Wiley & Sons, Ltd., 2019, pp. 25–45, <http://dx.doi.org/10.1002/9781119649182.ch2>.
- [18] N.C. Perkins, C.D. Mote, Comments on curve veering in eigenvalue problems, *J. Sound Vib.* 106 (1986) 451–463.
- [19] E.G. Williams, P. Roux, M. Rupin, W.A. Kuperman, Theory of multiresonant metamaterials for A_0 lamb waves, *Phys. Rev. B* 91 (2015) 104307.
- [20] A. Colombi, R. Craster, D. Colquitt, Y. Achaoui, S. Guenneau, P. Roux, M. Rupin, Elastic wave control beyond band-gaps: Shaping the flow of waves in plates and half-spaces with subwavelength resonant rods, *Front. Mech. Eng.* 3 (2017) 10, <http://dx.doi.org/10.3389/fmech.2017.00010>.
- [21] J. Maxwell, *Problems*, *Camb. Dublin Math. J.* 8 (1853) 188.
- [22] M. Dubois, M. Farhat, E. Bossy, S. Enoch, S. Guenneau, P. Sebbah, Flat lens for pulse focusing of elastic waves in thin plates, *Appl. Phys. Lett.* 103 (7) (2013).
- [23] R.K. Luneburg, M. Herzberger, *Mathematical Theory of Optics*, first ed., University of California Press, 1964.
- [24] M. Sarbort, T. Tyc, Spherical media and geodesic lenses in geometrical optics, *J. Opt.* 14 (7) (2012) 075705.
- [25] A. Colombi, Resonant metalenses for flexural waves in plates, *J. Acoust. Soc. Am.* 140 (5) (2016) EL423–EL428.
- [26] D. Torrent, Y. Pennec, B. Djafari-Rouhani, Effective medium theory for elastic metamaterials in thin elastic plates, *Phys. Rev. B* 90 (2014) 104110.
- [27] A. Climente, D. Torrent, J. Sánchez-Dehesa, Gradient index lenses for flexural waves based on thickness variations, *Appl. Phys. Lett.* 105 (2014) 064101.
- [28] Y. Jin, D. Torrent, Y. Pennec, Y. Pan, B. Djafari-Rouhani, Simultaneous control of the S_0 and A_0 lamb modes by graded phononic crystal plates, *J. Appl. Phys.* 117 (24) (2015).
- [29] L. Pomot, C. Payan, M. Remillieux, S. Guenneau, Acoustic cloaking: Geometric transform, homogenization and a genetic algorithm, *Wave Motion* 92 (2020) 102413, <http://dx.doi.org/10.1016/j.wavemoti.2019.102413>.
- [30] V. Krylov, Acoustic black holes: recent developments in the theory and applications, *IEEE Trans. Ultrason. Ferroelectr. Freq. Control* 61 (8) (2014) 1296–1306.
- [31] A. Palermo, A. Marzani, Control of Love waves by resonant metasurfaces, *Sci. Rep.* 8 (-) (2018) 7234.
- [32] A. Sharma, D.V. Kumar, A.K. Ghatak, Tracing rays through graded-index media: A new method, *Appl. Opt.* 21 (6) (1982) 984–987.
- [33] N.T. Aboulkhair, N.M. Everitt, I. Maskery, I. Ashcroft, C. Tuck, Selective laser melting of aluminum alloys, *MRS Bull.* 42 (4) (2017) 311–319.